A comprehensive experimental and modeling study of 2-methylbutanol combustion

ARTICLE *in* COMBUSTION AND FLAME · FEBRUARY 2015

Impact Factor: 3.08 · DOI: 10.1016/j.combustflame.2015.01.014

8 AUTHORS, INCLUDING:

Sungwoo Park
King Abdullah University of Science and Te…
9 PUBLICATIONS **50** CITATIONS
SEE PROFILE

Ossama Mannaa
King Abdullah University of Science and Te…
2 PUBLICATIONS **2** CITATIONS
SEE PROFILE

Fethi Khaled
King Abdullah University of Science and Te…
9 PUBLICATIONS **23** CITATIONS
SEE PROFILE

Morkous S. Mansour
King Abdullah University of Science and Te…
33 PUBLICATIONS **461** CITATIONS
SEE PROFILE

Combustion and Flame 162 (2015) 2166–2176

Contents lists available at ScienceDirect

Combustion and Flame

journal homepage: www.elsevier.com/locate/combustflame

A comprehensive experimental and modeling study of 2-methylbutanol combustion

Sungwoo Park [a,*], Ossama Mannaa [a], Fethi Khaled [a], Rafik Bougacha [a,b], Morkous S. Mansour [a,c], Aamir Farooq [a], Suk Ho Chung [a], S. Mani Sarathy [a,*]

[a] Clean Combustion Research Center, King Abdullah University of Science and Technology, Thuwal, Saudi Arabia
[b] Tunisia Polytechnic School, La Marsa, Tunisia
[c] Department of Mechanical Engineering, Helwan University, Cairo, Egypt

ARTICLE INFO

Article history:
Received 12 October 2014
Received in revised form 20 January 2015
Accepted 20 January 2015
Available online 20 February 2015

Keywords:
Chemical kinetic modeling
Shock tube
Constant volume combustion vessel
2-Methylbutanol
Ignition delay
Laminar flame speed

ABSTRACT

2-Methylbutanol (2-methyl-1-butanol) is one of several next-generation biofuels that can be used as an alternative fuel or blending component for combustion engines. This paper presents new experimental data for 2-methylbutanol, including ignition delay times in a high-pressure shock tube and premixed laminar flame speeds in a constant volume combustion vessel. Shock tube ignition delay times were measured for 2-methylbutanol/air mixtures at three equivalence ratios, temperatures ranging from 750 to 1250 K, and at nominal pressures near 20 and 40 bar. Laminar flame speed data were obtained using the spherically propagating premixed flame configuration at pressures of 1, 2, and 5 bar. A detailed chemical kinetic model for 2-methylbutanol oxidation was developed including high- and low-temperature chemistry based on previous modeling studies on butanol and pentanol isomers. The proposed model was tested against new and existing experimental data at pressures of 1–40 atm, temperatures of 740–1636 K, equivalence ratios of 0.25–2.0. Reaction path and sensitivity analyses were conducted for identifying key reactions at various combustion conditions, and to obtain better understanding of the combustion characteristics of larger alcohols.

1. Introduction

In recent years, the interest in alternative fuels has increased due to more stringent emission regulations and health concerns related to combustion of traditional fuels. Oxygenated fuels have been considered as potentially attractive alternative fuels, or fuel additives, to fossil fuels in order to reduce NO_x and particulate emissions [1]. In addition, the production of oxygenated fuels from renewable sources can offset CO_2 emissions from combustion devices. However, the combustion characteristics of oxygenated fuels need to be evaluated to determine advantages and disadvantages in the context of practical applications. Some oxygenated fuels can be used directly, while others need to be blended with traditional fuels prior to entering the combustor [2]. Ethanol, a first generation biofuel, is an attractive alternative bio-based alcohol fuel and can be used as a fuel extender for petroleum fuels. However, disadvantages such as high O/C ratio, high hygroscopicity, and low energy density can be problems with fuel storage, blending, and use in combustion engines. Therefore, the higher alcohol fuels, such as C_4 and C_5 alcohols, have been studied as next-generation biofuels. Recently, extensive combustion chemistry studies on butanol isomers [3–20] have been conducted and the focus of alcohol combustion research is shifting towards the C_5 family of alcohols, including *n*-pentanol [21–26], *iso*-pentanol (3-methyl-1-butanol) [27–31], and 2-methylbutanol (2-methyl-1-butanol) [32–35] because the longer chain alcohols are better suited for the use in combustion engines.

The interest for using 2-methylbutanol as a bio-derived fuel candidate has increased because it can be produced from various substrates by modified *Escherichia coli* bacteria [36] and photosynthesis by cyanobacteria [37]. However, there have been limited studies on 2-methylbutanol combustion. Tang et al. [24] measured the high temperature ignition behavior of C_5 alcohols (*n*-pentanol, *iso*-pentanol, and 2-methylbutanol) in the temperature ranging from 1100 to 1500 K and pressures of 1.0 and 2.6 atm. The ignition delay time and the global activation energy of the three isomers both decreased in the order of *iso*-pentanol, 2-methylbutanol, and *n*-pentanol. A high temperature chemical kinetic model for 2-methylbutanol was proposed and compared against their

* Corresponding authors at: Clean Combustion Research Center, King Abdullah University of Science and Technology, Thuwal 23955-6900, Saudi Arabia.
E-mail addresses: sungwoo.park@kaust.edu.sa (S. Park), mani.sarathy@kaust.edu.sa (S.M. Sarathy).

http://dx.doi.org/10.1016/j.combustflame.2015.01.014
0010-2180/

ignition data. Li and co-workers [32] measured laminar flame speeds of 2-methylbutanol/air mixtures at temperatures of 393, 433, and 473 K and pressures of 0.1, 0.25, 0.5, and 0.75 MPa using the spherically propagating flame. Experimental results showed that 2-methylbutanol has close laminar flame speeds with *n*-butanol. Zhao et al. [22] calculated pressure and temperature dependent rate constants for the thermal decomposition of *n*-pentanol and its isomers. Serinyel et al. [33] measured the concentrations of reactants, products, and intermediate species at a pressure of 10 atm, equivalence ratios of 0.5, 1, 2 and 4, and temperature ranging from 700 to 1200 K in a jet-stirred reactor (JSR) using GC and FTIR, and simulated their measurements using a detailed chemical kinetic mechanism. Recently, Zhang et al. [34] measured pyrolysis species of 2-methylbutanol in a flow reactor using synchrotron vacuum ultraviolet photoionization mass spectrometry at low and atmospheric pressures and tested a kinetic model against their measurements. The results indicate that the decomposition of 2-methylbutanol is similar to *iso*-butanol rather than *n*-butanol. Lucassen and co-workers [35] investigated the combustion chemistry of 2-methylbutanol in low-pressure premixed flames using flame-sampling molecular-beam mass spectrometry. Experimental data were compared with a detailed high-temperature chemistry to identify important fuel consumption pathways in the combustion of 2-methylbutanol.

The purpose of the present study is to expand experimental data available for 2-methylbutanol combustion at a broader range of conditions, in order to improve the mechanistic understanding of its combustion using a detailed chemical kinetic modeling. This study presents a comprehensive experimental dataset for 2-methylbutanol oxidation over a wide range of temperatures, pressures, and equivalence ratios. A comprehensive chemical kinetic model for 2-methylbutanol was developed using the rate rules established for modeling studies on other C_4 and C_5 alcohols. The model is compared against recently published experimental data, as well as new data presented herein. To our knowledge, this experimental and modeling study is the first to address the low-temperature and intermediate-temperature reactivity of 2-methybutanol.

2. Chemical kinetic model

The detailed chemical kinetic model for 2-methylbutanol includes both low- and high-temperature chemistry. The proposed model is based on previous alcohol modeling studies [1] of the C_4-alcohols [13], *n*-pentanol [23], and *iso*-pentanol [31], and a similar methodology was used in this study to develop a detailed chemistry model for 2-methylbutanol. For this work, the *iso*-pentanol model [31] has been extended by adding 109 species and 429 reactions to represent the combustion chemistry of 2-methylbutanol and its various intermediate species. Only a brief description of the model development is discussed herein. Most reaction classes and rate parameters follow directly from previous butanol isomers modeling work, as described by Sarathy et al. [1,13] and in Supplementary Material of [13]. It should be noted that the methods utilized for kinetic modeling of larger alcohols are approximations due to the lack of fundamental kinetic data. Therefore, the proposed model is an initial attempt at comprehensively modeling combustion of a complex alcohol fuel, for which significant basic research is needed to improve the underlying chemical fidelity.

To illustrate the naming of the species for the 2-methylbutanol mechanism, 2-methylbutanol is denoted as c5h11oh-2 in the mechanism (see Fig. 1 for its molecular structure). The carbon sites are labeled alphabetically (i.e., a, b, c, d, and e) to denote radical sites in the molecule. In this way, the β-hydroxypentyl radical at the tertiary site is denoted as c5h10oh-2b, while the

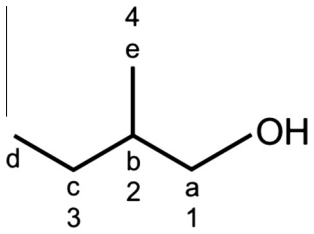

Fig. 1. Structure of 2-methylbutanol (c5h11oh-2) with carbon sites labeled.

α-hydroxypentyl radical is written as c5h10oh-2a. Additionally, the carbon chain is labeled numerically (i.e., 1, 2, 3, and 4) and the location of a double bond is identified by a hyphen followed by the number of the first carbon in the double bond (e.g., 2-methyl-1-butenol is c5h9oh21-1).

The major classes of elementary reactions considered for the oxidation of 2-methylbutanol are as follows:

High-temperature reaction classes

1. Unimolecular fuel decomposition.
2. H-atom abstraction from the fuel.
3. Fuel radical decomposition.
4. Fuel radical isomerization.
5. H-atom abstraction reactions from enols (i.e., unsaturated alcohols).
6. Enol-Keto tautomerizations and isomerizations catalyzed by H, HO_2, and formic acid.
7. Addition of H atoms to enols.
8. Enol radical decomposition.
9. Unimolecular decomposition of enols.
10. Reaction of O_2 with α-hydroxypentyl radicals to directly form an aldehyde + HO_2.

Low-temperature reaction classes (R refers to a 2-methylbutanol radical such as $C_2H_5C{\cdot}(CH_3)CH_2OH$ and QOOH refers to a hydroxypentyl hydroperoxide radical such as $C_2H_5C(OOH)(CH_3)C{\cdot}HOH$)

11. Addition of O_2 to fuel radicals (R + O_2 = ROO).
12. R + ROO = RO + RO.
13. R + HO_2 = RO + OH.
14. R + CH_3O_2 = RO + CH_3O.
15. ROO radical isomerization (ROO = QOOH) including Waddington type reaction mechanism.
16. Concerted eliminations (ROO = enol + HO_2).
17. ROO + HO_2 = ROOH + OH.
18. ROO + H_2O_2 = ROOH + HO_2.
19. ROO + CH_3O_2 = RO + CH_3O + O_2.
20. ROO + ROO = RO + RO + O_2.
21. ROOH = RO + OH.
22. RO decomposition.
23. Formation epoxy alcohols via cyclization.
24. QOOH = enol + HO_2 (radical site beta to OOH group).
25. QOOH = alkene/enol + carbonyl + OH (radical site gamma to OOH group) including unconventional water elimination reaction.
26. Addition of O_2 to QOOH (QOOH + O_2 = OOQOOH).
27. Reaction of O_2 with α-hydroxypentyl hydroperoxide radicals (e.g., $C_2H_5C(OOH)(CH_3)C{\cdot}HOH$ + O_2).
28. Isomerization of OOQOOH and formation of carbonyl hydroxypentyl hydroperoxide species and OH including Waddington type reactions mechanisms.
29. Decomposition of carbonyl hydroxypentyl hydroperoxide species to form oxygenated radical species and OH.

30. Cyclic oxygenates reactions with OH and HO_2.

The reaction of α-hydroxypentyl radical with O_2 can proceed through an activated α-hydroxypentyl peroxy adduct that rapidly decomposes to 2-methylbutanal and HO_2. The decomposition reaction occurs with such a low barrier that it essentially inhibits the low-temperature ignition behavior of alcohols. There are no fundamental studies on larger alcohols to determine whether the aforementioned reaction sequence occurs as a single concerted reaction step or via a stabilized α-hydroxypentyl peroxy adduct. In the present study, we assume the former and include this reaction as a high-temperature reaction class 10 (i.e., α-hydroxypentyl radicals reactions with O_2) and uses the same modified pressure dependent rate constants as the *iso*-pentanol modeling study [31] to better capture the low-temperature ignition delay reactivity. Specifically, the high-pressure limit was decreased by a factor of 2.5, while the rate constant at all other pressures was increased by a factor of 2.5. This rate constant modification is within the uncertainty limits of the original rate estimation, which is from previous work on n-butanol [13] and tested against a limited set of data. The uncertainties in rate constants and branching ratios of various pathways on the $R + O_2$ potential energy surface are rather large for C_4 and larger alcohols because these systems have not been subject to quantitative experimental or theoretical studies. The same modified rate constant for reaction class 27 (i.e., α-hydroxypentyl hydroperoxide radicals reactions with O_2) was also employed to keep it in agreement with the rate constant for reaction class 10.

Pressure dependent rate constants for unimolecular decomposition of 2-methylbutanol were obtained from analogy with the decomposition of the butanol isomers [13], which is based on the location of the bond scission (i.e. *iso*-butanol rates were adopted for secondary-tertiary and primary-tertiary scission, and other scissions adopted *n*-butanol or *sec*-butanol rates with respect to the bond scission location). The recently updated pressure dependent reaction rate coefficients for the thermal decomposition of *iso*-butanol by Zhou et al. [38] were adopted for the C–C bond dissociation near methyl branch; however, the rate constant leading to 2-butyl and hydroxymethyl radicals was increased by a factor of five to enhance the high-temperature reactivity, which is based on a sensitivity analysis discussed later.

The model includes the Waddington reaction pathway [39,40] involving the internal H-atom migration of from the OH group to the β-hydroxypentyl peroxy (β-ROO) radical via 6-membered transition state ring, followed subsequent rapid decomposition to produce 2-butanone, formaldehyde, and OH. Similar pathways proposed by Welz et al. [41] were also adopted in this study for H-atom transfer in γ- and δ-hydroxypentyl peroxy (ROO) radicals via 7- and 8-member transition state rings. Welz and co-workers [42] presented an unconventional water elimination reaction from hydroxypentyl hydroperoxide (QOOH) radicals, and the present model added this reaction pathway as an irreversible reaction with an activation energy 10 kcal mol^{-1} lower than β–decomposition of QOOH radicals [31].

The thermodynamic data for 2-methylbutanol and radicals were calculated using THERM program of Ritter and Bozzelli [43]. For transport properties, the correlations developed by Tee et al. [44] were used to calculate the Lennard-Jones (LJ) collision diameter and potential energy well depth using the critical pressure (p_c), critical temperature (T_c), and acentric factor (ω). All the simulations were conducted in CHEMKIN PRO 15112 [45] using appropriate reactor modules. The simulation for the laminar burning velocities was performed with the PREMIX module in CHEMKIN PRO [45] and the simulations accounted for thermal diffusion (i.e., Soret effect), assumed mixture-averaged transport, and the solutions were highly resolved with approximately 200 grid points (GRAD 0.1, CURV 0.1). The present model consists of 469 species and 2504 reactions and the CHEMKIN input files are provided in Supplementary material and on the website http://cpc.kaust.edu.sa.

2.1. Model validation studies

In this study, the proposed model for 2-methylbutanol is compared against a wide range of experimental data. Note, the high-temperature sub-chemistry for 2-methylbutanol has been previously compared with low-pressure premixed flame data [35]. The following is a list of specific targets considered in this study:

1. Published [24] ignition delay time data from a shock tube at Xi'an Jiaotong University over a temperature range of 1175–1636 K, pressure of 1 atm, and equivalence ratios of 0.25, 0.5 and 1.0.
2. New ignition data from a shock tube at KAUST at equivalence ratios of 0.5, 1.0 and 2.0 in air, temperatures from 950 to 1250 K, and a nominal pressure of 20 bar.
3. New ignition data from a shock tube at KAUST at equivalence ratios of 0.5, 1.0 and 2.0 in air, temperatures from 750 to 1100 K, and a nominal pressure of 40 bar.
4. Published [32] premixed laminar flame speeds from a constant volume combustion chamber at Xi'an Jiaotong University.
5. New premixed laminar flame speed data from a constant volume combustion vessel at KAUST at temperatures of 353 K (373 K for 5 bar), equivalence ratios ranging from 0.7 to 1.5, and pressures of 1, 2, and 5 bar.
6. Published [33] concentration profiles from a JSR at CNRS Orleans operating at 10 atm, constant residence time of 0.7 s, equivalence ratio of 1.0, and temperatures from 740 to 1190 K.

3. Experimental methodologies

3.1. Shock tube facility

The high-pressure shock tube (HPST) used for this work is a 13.2 m long stainless steel tube with a 10 cm internal diameter. The driven section is 6.6 m long and the driver section length can be varied up to a maximum of 6.6 m. A mid-section is used in the HPST between the driver section and the driven section to allow better control of the post-reflected shock conditions. Two cross-scored aluminum diaphragms are used in the mid-section. Aluminum grade, thickness, and scoring depth of the diaphragms are carefully selected to reach the desired temperature and pressure conditions behind the reflected shock wave. Five axially-spaced PCB 113B26 piezoelectric pressure transducers (PZTs) were placed in the last 1.3 m of the driven section for measurement of the incident-shock velocity. Each PZT is mounted such that its surface is recessed approximately 1 mm from the inner diameter of the shock tube and the PZT surface is coated with a thin (~1 mm) layer of red silicon RTV to protect the pressure sensor from thermal shock. The signals from PZTs are used to trigger five ultrafast (350 MHz) Agilent 53220A frequency counters to determine the time interval between two successive pressure transducers. Incident shock attenuation rates vary from 0.2 to 1.8%/m. Shock jump relations and known thermodynamic parameters are then used to calculate the post-reflected shock conditions (P_5 and T_5). Uncertainty in the incident-shock velocity determination at the driven-section endwall leads to uncertainties of less than 1% in both the reflected-shock temperatures and pressures at the measurement location. Sidewall pressure traces are measured using a Kistler 603B1 PZT located at 1.0 cm from the endwall. Additionally, OH^* chemiluminescence at 307 nm is monitored at the endwall and sidewall (1.0 cm from the endwall) ports (with sapphire windows) using PDA36A photo-detectors. The spectral

response range of this photo-detector is 350–1100 nm. Hence, the photodiode of PDA36A was swapped with a Silicon photodiode (type S1722-02 Hamamatsu). The modified photo-detector is sensitive over 190–1100 nm and provides good response for OH* emission.

Fuel/air mixtures are prepared in a gas-mixing facility consisting of two 40-liter magnetically-stirred stainless-steel mixing tanks. After pumping the mixing tank to pressures less than 10^{-4} mbar, 2-methylbutanol is injected directly in the heated mixing tank. The injection is made through a septa rubber valve that has high sealing properties. The mixing tank and manifold are both equipped with electrical heating elements to prevent condensation of 2-methylbutanol, which has relatively low vapor pressure (~4 mbar at 25 °C). Hence, extreme precautions have to be taken to prevent condensation of the fuel. For the experiments described here, both the mixing tank and manifold were electrically heated to approximately 110 °C. At this temperature, the saturation vapor pressure of 2-methylbutanol is at least 1.5 times the partial pressure used in the mixture. Furthermore, a He-Ne laser beam at 3.39 μm is used to monitor the fuel concentration inside the shock tube prior to each run. For this purpose, separate measurements in a static stainless steel cell were carried out to calculate the absorption cross-section of 2-methylbutanol at the conditions of these experiments. These static cell experiments led to a value of 3.65×10^{-19} cm^2/molecule for the absorption cross-section of 2-methylbutanol at 383 K. This value was used to calculate the fuel concentration prior to each shock by applying the Beer–Lambert law:

$$\ln\left(\frac{I}{I_0}\right) = \sigma NL \tag{1}$$

Here, I_0 and I are the laser beam intensity before and after filling the mixture inside the shock tube; σ is the absorption cross-section; N is the number density of 2-methylbutanol; L is the pathlength which is equal to the diameter (10 cm) of the shock tube. Measurements performed with He–Ne laser result in equivalence ratios that are within 4% of the manometrically measured values.

2-Methylbutanol was procured from Sigma Aldritch (99.9% purity). Research grade oxygen and nitrogen cylinders (99.999% purity) were purchased from Abdullah Hashim Gas Company. A molar ratio of 3.76:1 of N_2:O_2 is used to prepare fuel/air mixtures. Driver-gas tailoring (nitrogen in helium) was carried out with the help of two mass flow controllers to extend the shock tube test times to about 10 ms. A small pressure rise behind reflected shock wave (dP_5/dt) is observed which varied from 2%/ms to 3%/ms.

Ignition delay time measurements were carried out at three equivalence ratios (0.5, 1 and 2) and at two nominal pressures (20 and 40 bar). Reflected shock temperatures ranged 950–1250 K for 20 bar experiments and 750–1100 K for 40 bar data. Mixtures compositions used for fuel rich, lean, and stoichiometric experiments are summarized in Table 1. An example ignition delay time measurement is shown in Fig. 2. Time zero was defined as the time of mid-point of pressure jump from P_2 (pressure behind the incident shock wave) to P_5 (pressure behind the reflected shock wave). The onset of ignition is detected by the maximum slope in the sudden increase of pressure and OH* chemiluminescence; the two signals result in very similar ignition delay times.

Table 1
Mixtures compositions for 2-methylbutanol ignition delay experiments.

Equivalence ratio	2-Methylbutanol (%)	Oxygen (%)	Nitrogen (%)
$\phi = 0.5$	1.38	20.72	77.90
$\phi = 1$	2.72	20.44	76.84
$\phi = 2$	5.30	19.9	74.80

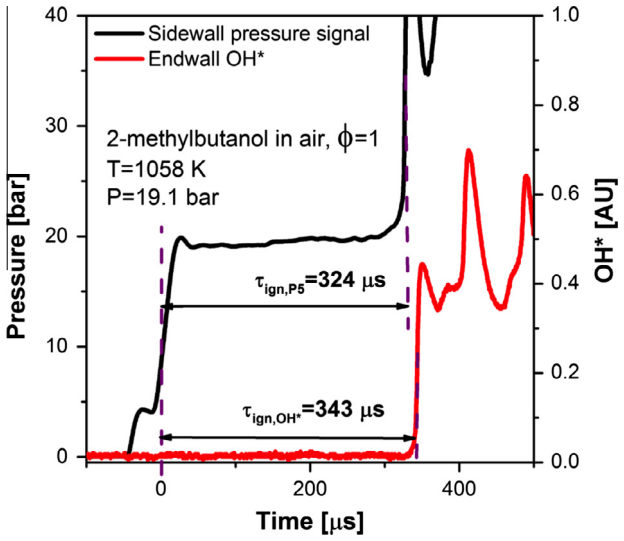

Fig. 2. Typical pressure and OH* trace during 2-methylbutanol ignition delay experiments.

Representative pressure and OH* signals are shown in Fig. 2. Ignition delay times investigated in this work ranged from 100 μs to 8 ms.

3.2. Constant volume combustion vessel

A spherical stainless steel combustion vessel with 330 mm inner diameter (≈20 liters) was utilized for laminar flame speed measurements. It has two orthogonal pairs of quartz windows with 120 mm diameter and 50 mm thickness, which is capable of withstanding the temperatures and pressures generated from deflagrations at initial pressures, P_o, of up to 0.7 MPa and initial temperatures, T_o, of up to 400 K. The vessel can accommodate both liquid and gaseous fuels and/or their blends. An electric heater (1 kW) located at inside of the bottom flange was heating the vessel and mixtures up to 400 K. The initial gas temperature was measured at two locations by sheathed Chromel–Alumel thermocouples with 1.5 mm diameter to assure thermal homogeneity of the mixtures. To improve the homogeneity of mixtures, a rotating fan was located inside the vessel at the top flange, which was driven by a magnet-electric motor. The convective heat transfer process was enhanced by turbulence generated from this fan which assured temperature uniformity throughout the vessel as well as improving liquid fuel evaporation. Reactants were prepared in the combustion vessel using the partial pressure method, assuming an ideal gas model. The volume of injected liquid fuel was calculated from the number of moles, being proportional to the partial pressure and its density. Liquid fuels were injected into the vessel under vacuum pressure of about 0.001 MPa then dry air was introduced according to initial conditions (ϕ, P_o, T_o). A pressure transducer (Keller; PAA-33X) monitored the partial pressure of reactants during mixture preparation as well as initial pressure before ignition. A second pressure transducer (Kistler; 6045A) measured pressure variations during flame propagation. Spherical flame images were captured by adopting schlieren cine-photography to determine the absolute flame speed, S_n. A high speed camera (Photron; FastCam Ultima APX 120 K) was used for image acquisition with 4000 fps and 512 × 512 pixels (0.317 mm/pixel resolution). The experimental repeatability was checked through three realizations at each experimental condition.

Absolute flame speed, S_n, was calculated, through direct measurements of the flame radius $R_f(t)$ extracted from the schlieren system.

$$S_n = \frac{dR_f}{dt} \quad (2)$$

Effects of flame stretch rate have to be considered for such spherical flame method, which result in the following expression:

$$\kappa = (2/R_f)S_n \quad (3)$$

Measurements were conducted during an earlier stage of flame propagation to assure near constant pressure regime. From the measured S_n, the stretched flame speed, S, free from perturbation due to ignition transient or instability by developing cellular structure, was selected. The un-stretched laminar burning velocity, S_o, was determined from the following linear extrapolation to zero stretch:

$$S_o - S = L_b\kappa \quad (4)$$

where L_b is the Markstein length of burnt gas. Eq. (4) is applicable as the flame is assumed to be thin, and both buoyancy and radiative losses effects are negligible [46]. In the constant pressure regime, the laminar burning velocity u_l can be obtained based on the mass conservation across the flame front according the following expression:

$$u_l = S_o(\rho_b/\rho_u) \quad (5)$$

where ρ_b and ρ_u are the burnt and unburned gas densities, respectively.

A typical response of stretch flame propagation with respect to stretch rate is shown in Fig. 3. Initially (small flame radius and large stretch), the flame exhibits a large flame speed before attaining a minimum value as the flame is overdriven by spark energy. After recovering from the ignition-transient regime, the flame start its linear response with respect to stretch rate, which is used for linearly extrapolating the stretched flame speed to a zero stretch rate to obtain S_o. For high pressure rich flames, S_n increases significantly at later stages of propagation due to flame instability triggered by the development of cellular flame structure.

4. Results and discussions

4.1. Autoignition delay times

The proposed model is first compared against high-temperature shock tube ignition data obtained by Tang et al. [24]. The experiments were conducted over a temperature range of 1175–1636 K, pressure of 1 atm, and equivalence ratio of 0.25, 0.5, and 1.0. Fuel/O_2 mixtures were highly diluted by Ar and the 2-methylbutanol concentration was maintained at 0.5 mol%. Figure 4 presents the experimental data along with computed ignition delay times at 1 atm for three equivalence ratios. In the simulations, the onset of ignition is the time corresponding to the maximum rate of temperature rise (max dT/dt), which corresponds closely to the maximum pressure rise rate (max dP/dt). The model agrees with experimental data and reproduces the experimental trend of increasing ignition delay time with increasing equivalence ratio. This trend is consistently observed in the high-temperature ignition of hydrocarbons where the reactivity is driven by H + O_2 = OH + O chain branching reaction. The decrease of O_2 concentration with an increase of equivalence ratio leads to a decrease of the rate of the chain branching reaction and an increase in ignition delay time. In addition, H radicals are consumed by fuel + H abstraction reactions under rich conditions, thus inhibiting their participation in the aforementioned chain branching reaction. Figure 3 also shows that the present model captures the experimental activation energy better than the model proposed by Tang et al. [24].

New ignition delay times for 2-methylbutanol/air mixtures were measured using the HPST at KAUST over a temperature range of 950–1250 K, equivalence ratios of 0.5, 1.0, and 2.0, and nominal pressures of 20 bar. The ignition delay times of 2-methylbutanol/air mixtures were compared to the *iso*-pentanol (3-methyl-1-butanol) ignition data measured by Tsujimura et al. [30] using a shock tube (ST) at NUI Galway, as shown in Fig. 5. It is interesting to note that the ignition delay times of 2-methylbutanol/air mixtures at intermediate temperatures (950–1050 K) are similar to those of *iso*-pentanol, but the reactivity of 2-methylbutanol is higher than *iso*-pentanol at high temperatures (T > 1050 K) (i.e., ignition delay

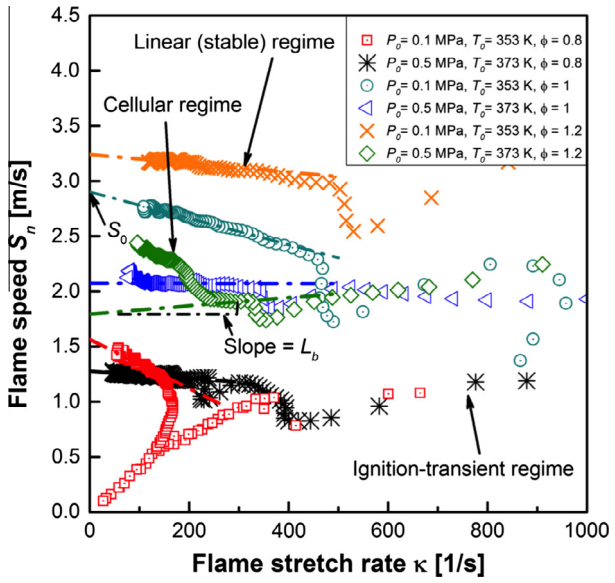

Fig. 3. Stretched flame propagation speeds with strain rate at different pressure and equivalence ratios.

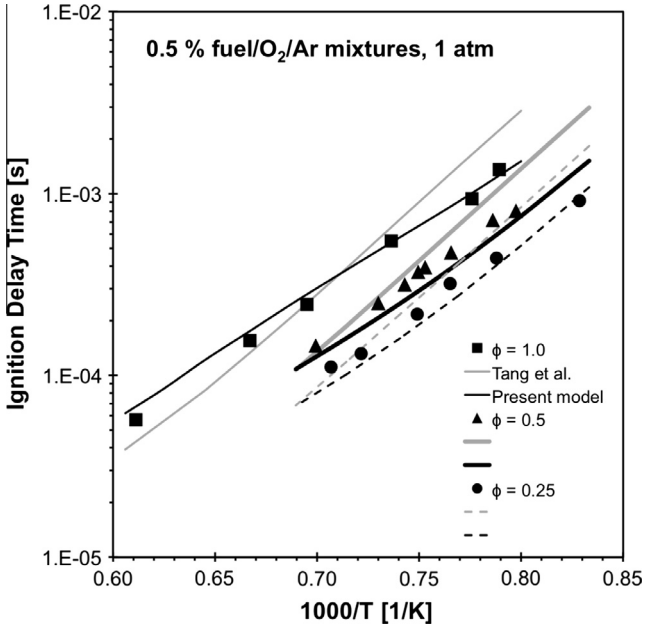

Fig. 4. Ignition delay times for 2-methylbutanol at 1 atm [24] compared with simulations using the model from Tang et al. [24] and the present work.

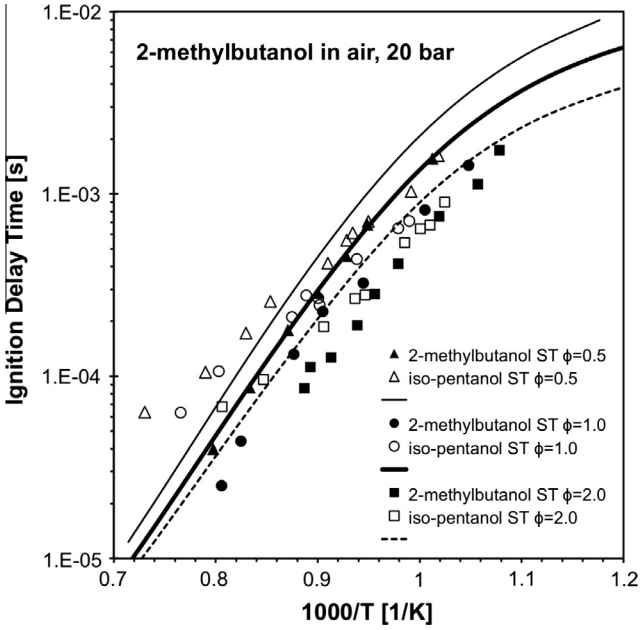

Fig. 5. HPST ignition delay times for 2-methylbutanol at 20 bar compared with iso-pentanol ST data and simulations.

times and overall activation energy of 2-methylbutanol are lower than *iso*-pentanol). The experimental results presented herein are consistent with high-temperature shock tube ignition data acquired by Tang et al. [24]. The present model is compared against the HPST ignition delay time data using the adiabatic homogenous reactor model in CHEMKIN PRO [45] with an imposed volume history determined using the variable volume method (VTIM) proposed by Chaos and Dryer [47] to account for the experimentally measured pressure gradient of $dP/dt(1/P_0) = 3\%$ per millisecond. Overall, the proposed model has a reasonable agreement with the HPST ignition data. The model over-estimates ignition delay time under these conditions with a maximum difference of about a factor of 2. The experimental data displays a decrease in ignition delay time as the equivalence ratio increases, and the trend is different to that observed previously in high-temperature ST conditions because the driving reactivity is different. The combination reaction $H + O_2 + M = HO_2 + M$ is dominant below 1200 K and increasing fuel concentration with increasing equivalence ratio results in increased radical production and increased overall reactivity, via fuel + HO_2 = fuel radical + H_2O_2 followed by $H_2O_2 + M = OH + OH + M$. The trend is well captured by the present model.

Figure 6 displays the dominant reaction pathways for the consumption of 2-methylbutanol at 1300 K, 20 bar, three equivalence ratios, and at time corresponding to 20% of the fuel consumed. At all equivalence ratios, unimolecular fuel decomposition to the formation of 2-butyl radical and hydroxymethyl radical is one of dominant fuel consumption pathways. The rate constant for this pathways is important for correctly simulating high-temperature reactivity, as it eventually leads to the formation of H radicals following β-decompositions of 2-butyl and hydroxymethyl radicals. H-atom abstraction reactions are also important at the given conditions, favoring the α-site due to its low C-H bond dissociation energy. Subsequently, β-scission of fuel radicals leads to the formation of smaller radicals and unsaturated species (e.g., alkenes, enols and/or aldehydes) in favor of C–C or C–O bond cleavage. Propene

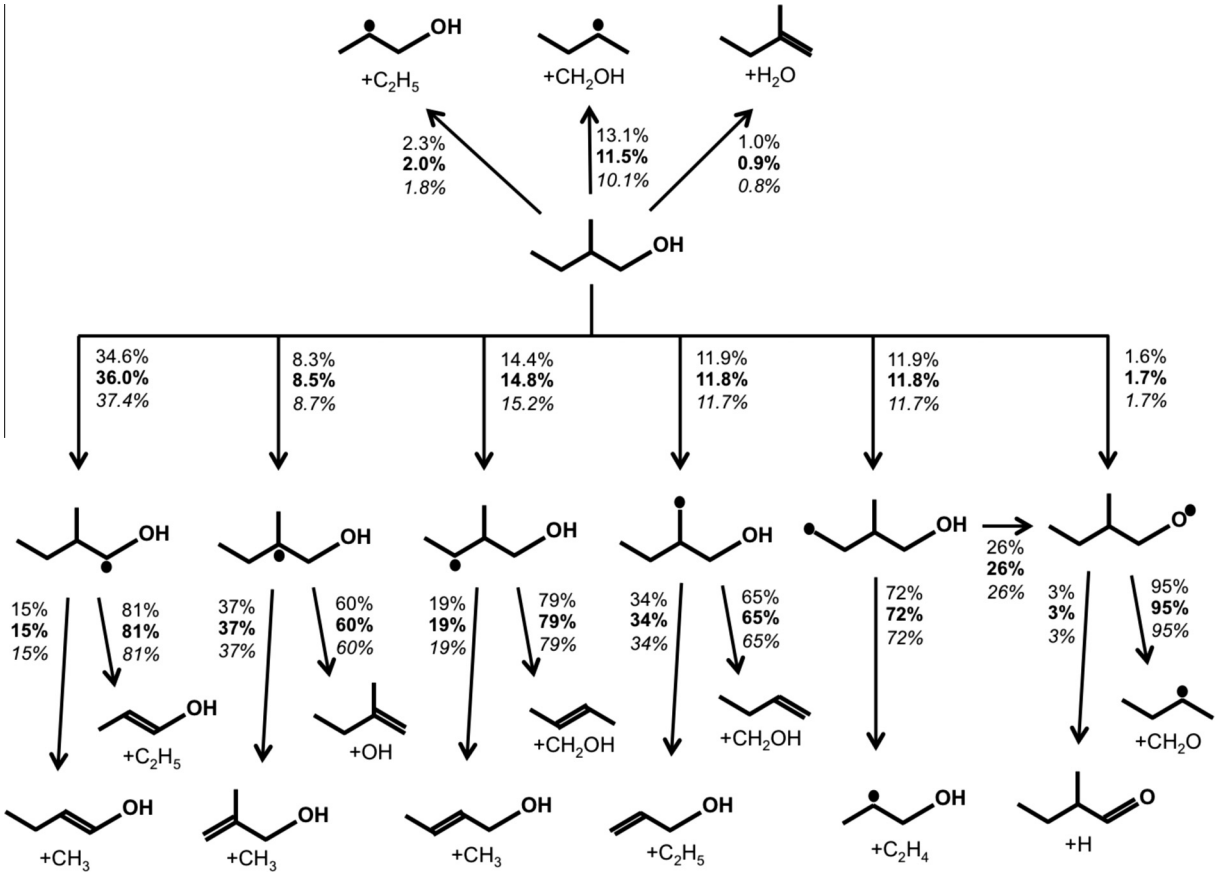

Fig. 6. Reaction path analysis for 2-methylbutanol at 1300 K, 20 bar, $\phi = 0.5$ (plain), $\phi = 1.0$ (bold) and $\phi = 2.0$ (italic). The reaction fluxes are given at 20% fuel consumption.

and *iso*-butene are major intermediate species of *iso*-pentanol radical β-scissions [31], while ethylene and butene isomers (1-butene, 2-butene) are major intermediate species of 2-methylbutanol combustion (i.e. $C{\cdot}H_2CH_2CH(CH_3)CH_2OH = C_2H_4 + CH_3C{\cdot}HCH_2OH$, $CH_3C{\cdot}HCH(CH_3)CH_2OH = 2\text{-}C_4H_8 + CH_2OH$ and $CH_3CH_2CH(C{\cdot}H_2)CH_2OH = 1\text{-}C_4H_8 + CH_2OH$).

Figure 7 presents the sensitivity coefficients obtained through a brute force sensitivity analysis for ignition delay time at 20 bar and 1300 K. This was preceded by a temperature sensitivity analysis at the time of ignition to identify the important reactions for subsequent consideration in the brute force sensitivity analysis. Previous work has shown that a temperature sensitivity analysis identifies the same reactions as a brute force sensitivity analysis, albeit the latter method provides sensitivity coefficients that are more meaningful [31]. The sensitivity coefficients of selected reaction steps were computed by the formula $\sigma = \log(\tau+/\tau-)/\log(2.0/0.5)$ where $\tau+$ and $\tau-$ are the computed ignition delay times corresponding to an increase and a decrease by a factor two of a rate coefficient [48,49]. Therefore, positive sensitivities represent an increase in the ignition delay when the reaction rate coefficient is increased. The most sensitive reaction is the thermal decomposition reaction of 2-methylbutanol leading to the formation of 2-butyl radical and hydroxymethyl radical, and the analysis indicates that the reaction becomes more sensitive at larger equivalence ratio. Therefore, a change in this reaction rate coefficient will have a greater effect on high-temperature reactivity at higher equivalence ratios. The reaction of methyl radical with HO_2 is the next most sensitive reactions at high temperatures, wherein the route to methoxy and OH radicals has a negative value, while the route to methane and O_2 has a positive one. The former is a chain propagating pathway, while the latter is a chain terminating one. The analysis also shows that the high-temperature reactivity is largely driven by the chain branching reaction $H + O_2 = OH + O$. In addition, reactions involving ethylene and propenyl also have a significant effect on 2-methylbutanol ignition at high temperatures.

The model was also compared against new ignition delay time data of 2-methylbutanol/air mixtures obtained near 40 bar using the HPST at KAUST over a temperature range of 750–1100 K,

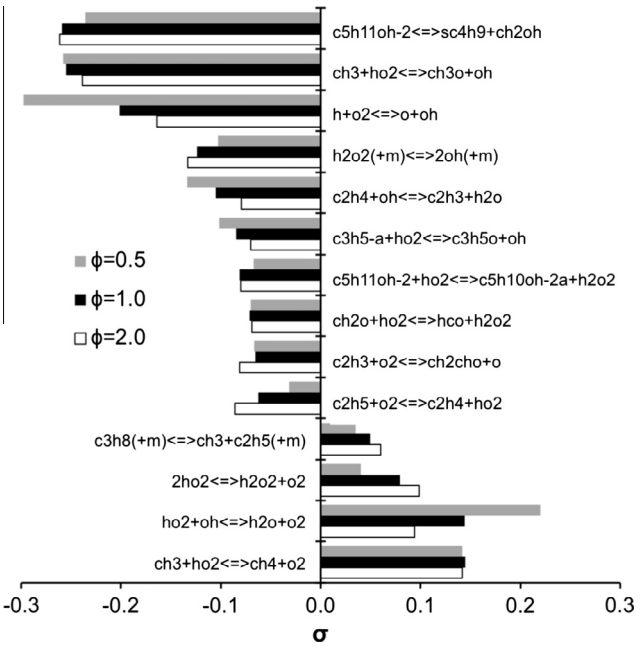

Fig. 7. Brute force sensitivity analysis for ignition delay time with respect to reaction rate coefficients for 1300 K, 20 bar and ϕ = 0.5, 1.0 and 2.0.

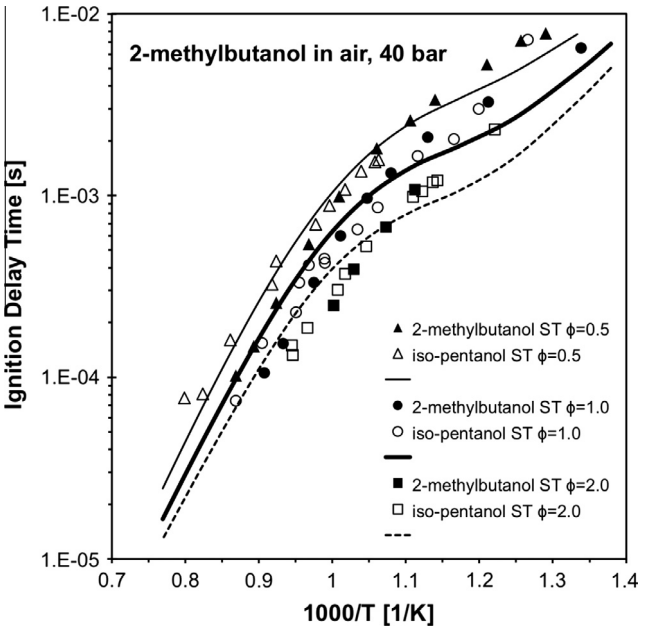

Fig. 8. HPST ignition delay times for 2-methylbutanol at 40 bar compared with iso-pentanol ST data and simulations.

equivalence ratios of 0.5, 1.0, and 2.0, as shown in Fig. 8. Simulations were carried out using the adiabatic homogenous reactor model in CHEMKIN PRO [45] with an imposed volume history to account for the experimentally measured pressure gradient of $dP/dt(1/P_0) = 3\%$ per millisecond. Ignition delay time data for equivalence ratio of 2.0 are limited because the low-vapor pressure of 2-methylbutanol prohibits high fuel loading needed for rich fuel/air mixtures. Ignition delay times of 2-methylbutanol/air mixtures were also compared with *iso*-pentanol ignition data measured in the ST at Rensselaer Polytechnic Institute [31]. The trend previously observed at 20 bar is also observed at 40 bar conditions, specifically that ignition delay times of both fuel/air mixtures are similar at intermediate temperatures, while 2-methylbutanol is more reactive at higher temperatures. The HPST ignition data of 2-methylbutanol/air mixtures are very close to *iso*-pentanol/air ST data in the intermediate temperature region (800–1000 K). The proposed model reproduces the ST ignition delay data and overall activation energy over the entire temperature range at 40 bar with a maximum deviation of 50% at low temperatures. The present model also captures the trend of decreasing ignition delay time with increasing equivalence ratio.

The reaction path analysis of 2-methylbutanol/air mixtures at initial conditions of 800 K, 40 bar, and three equivalence ratios are shown in Fig. 9 for the time corresponding to 20% fuel consumption. The fuel is mainly consumed by H-atom abstraction reactions in favor of the α-site because of the weak C–H bond dissociation energy. Subsequently, α-hydroxypentyl radical reacts with molecular oxygen to produce 2-methylbutanal and HO_2, which is a low-temperature chain terminating pathway [50]. The other fuel radicals add O_2 at radical sites to produce hydroxypentyl peroxy (ROO) radicals. As expected, β-scission decomposition of fuel radicals increases with increasing equivalence ratios due to the lack of O_2. The hydroxypentyl peroxy (ROO) radicals mainly undergo isomerization to form hydroxypentyl hydroperoxide (QOOH), except for the β-hydroxypentyl peroxy (β-ROO) radical with the peroxy group at the tertiary site. Around 29% of β-hydroxypentyl peroxy radicals are decomposed to produce enol species and HO_2 (i.e., concerted elimination) and 17% to 2-butanone, formaldehyde, and OH radical via the Waddington mechanism

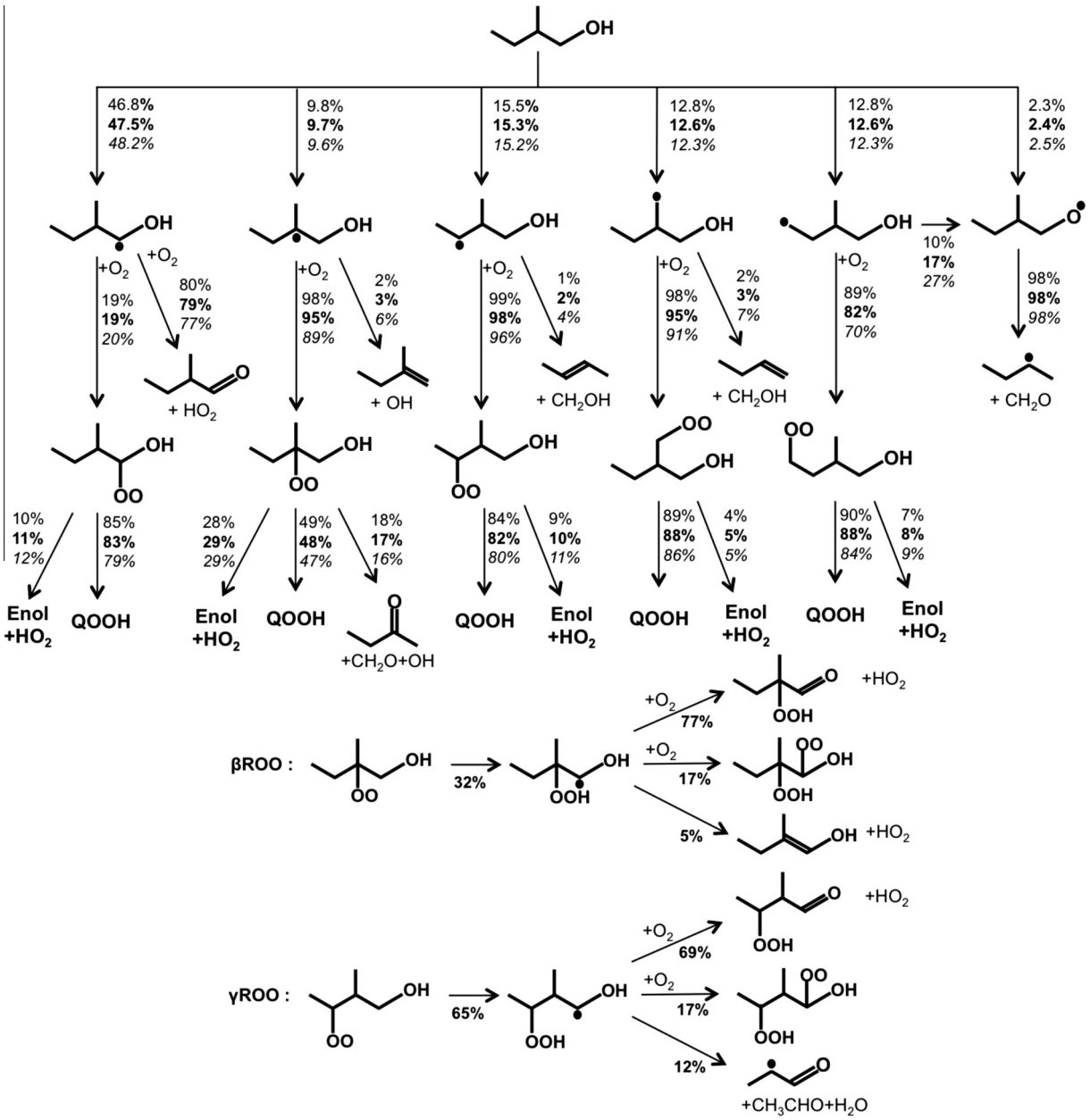

Fig. 9. Reaction path analysis for 2-methylbutanol at 800 K, 40 bar, ϕ = 0.5 (plain), ϕ = 1.0 (bold) and ϕ = 2.0 (italic). The reaction fluxes are given at 20% fuel consumption.

[39,40]. The other hydroxypentyl peroxy radicals undergo typical low-temperature chain branching reactions.

Additional reaction pathways are also presented in Fig. 9 for the α-hydroxypentyl hydroperoxide radical produced from isomerization of the β-hydroxypentyl peroxy radical. The α-hydroxypentyl hydroperoxide radical reacts with O_2 to form HO_2 radical and hydroperoxide pentaldehyde, which decomposes to form OH radical. Therefore, this reaction pathway produces one OH and one HO_2 radical in the low-temperature scheme. Only 17% of α-hydroxypentyl hydroperoxide radicals produced from β-hydroxypentyl peroxy (β-ROO) radicals add O_2 to the radical site (second O_2 addition) to produce OOQOOH radicals. Conventional low-temperature chain branching reactions are inhibited because the 5-member ring internal H-atom migration reactions are not possible due to the presence of methyl branch (i.e., there is no available C–H bond at the tertiary site carbon atom bonded to the hydroperoxide (OOH) group). In addition, the fate of the α-hydroxypentyl hydroperoxide radical produced from the γ-hydroxypentyl peroxy (γ-ROO) radical is presented in Fig. 9. The formation of hydroperoxide pentaldehyde and HO_2 is also a dominant pathway and around 12% of α-hydroxypentyl hydroperoxide undergoes the unconventional water elimination reaction proposed by Welz et al. [42].

In order to highlight the important reactions controlling the ignition of 2-methylbutanol/air mixtures, a brute force sensitivity analysis for selected reaction steps was conducted at 40 bar and 800 K, and for three equivalence ratio, as shown in Fig. 10. The reaction of α-hydroxypentyl radical with O_2 to form 2-methylbutanal and HO_2 has the greatest positive sensitivity. On the other hand, the channel forming α-hydroxypentyl peroxy (α-ROO) has a negative sensitivity. The former reaction leads to the low-temperature chain termination, while the latter leads to the low-temperature chain branching reactions. H-atom abstraction by OH radicals from the α-site also displays a high positive sensitivity because the α-hydroxypentyl radical that is produced ends in OH termination. Other H-atom abstraction reactions by OH radicals have negative sensitivities because these radicals lead to the

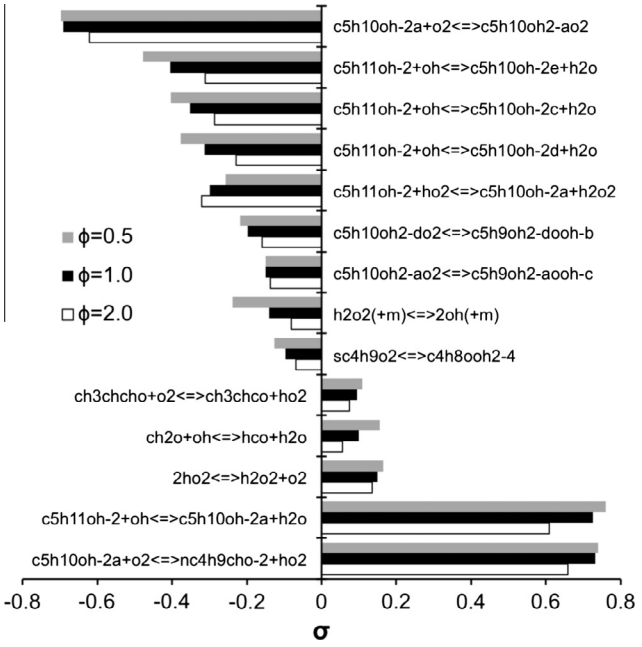

Fig. 10. Brute force sensitivity analysis for ignition delay time with respect to reaction rate coefficients for 800 K, 40 bar and ϕ = 0.5, 1.0 and 2.0.

low-temperature chain branching reaction pathways. The ignition delay is also sensitive to the isomerization of hydroxypentyl peroxy (ROO) radicals. This indicates that hydroxypentyl radicals undergo typical low-temperature chain branching reactions, except for the α-hydroxypentyl radical. It should be noted that H-atom abstraction by HO_2 radical to form α-hydroxypentyl has a negative sensitivity because H_2O_2 eventually decomposes to two OH radicals and increases the system reactivity. It is interesting that the isomerization of 2-butylperoxy radical has also negative sensitivity under these conditions. The 2-butyl radical can be produced from alkoxy radical ($C_2H_5CH(CH_3)CH_2O\cdot$) or 2-methylbutanal decompositions.

4.2. Laminar flame speeds

Li and co-workers [32] measured the laminar burning velocities of 2-methylbutanol/air mixtures from spherically propagating flames using a combustion chamber with an inner diameter of 180 mm and volume of 5.5 L at various pressures (1, 2.5, 5 and 7.5 bar) and temperature conditions (393, 433 and 473 K). The proposed model is compared against the data at 433 K and various pressure conditions, as shown in Fig. 11. Simulations on laminar burning velocity were conducted using the PREMIX flame code in CHEMKIN PRO [45]. A detailed high-temperature mechanism was used for these simulations, wherein reaction classes 1–10 were only used. The simulation includes thermal diffusion (i.e. Soret effect), mixture averaged transport properties, and the solutions were highly resolved with approximately 200 grid points (GRAD 0.1, CURV 0.1). Overall, the proposed model accurately simulates the experimental data. The model captures the stoichiometric laminar burning velocity data at atmospheric pressure, while slightly under-estimating in the fuel-lean region and over-estimating in the fuel-rich region. On the other hand, high-pressure experimental data are well captured by the model except for an over-estimation at 2.5 bar and equivalence ratios between 1.1 and 1.4. The results also show that the model well reproduces the experimentally observed trend that laminar burning velocities decrease as pressure increases. In general, the model has a better agreement at high pressures.

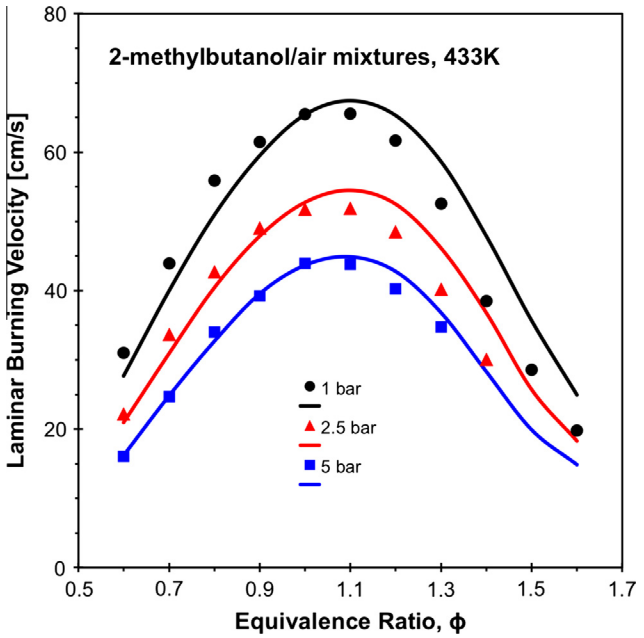

Fig. 11. Laminar flame speeds at unburnt gas temperature of 433 K and different pressures. Experimental data [32] (symbols) are compared to calculations (lines).

New laminar burning velocity data for 2-methylbutanol/air mixtures were at pressures of 1, 2, and 5 bar and a temperature of 353 K (373 K for 5 bar). Figure 12 presents the data along with existing *iso*-butanol [51] and *iso*-pentanol [31] data. It is interesting to note that the laminar burning velocities of 2-methylbutanol/air mixtures are similar to those of *iso*-butanol measured at Princeton [51] and *iso*-pentanol measured at USC [31] at the same unburnt gas temperature of 353 K. This result is consistent with laminar burning velocities of *n*-alkane fuels having similar structure but different chain length, as studied by Ji et al. [52]. 2-methylbutanol has a slightly faster flame speed than *iso*-butanol

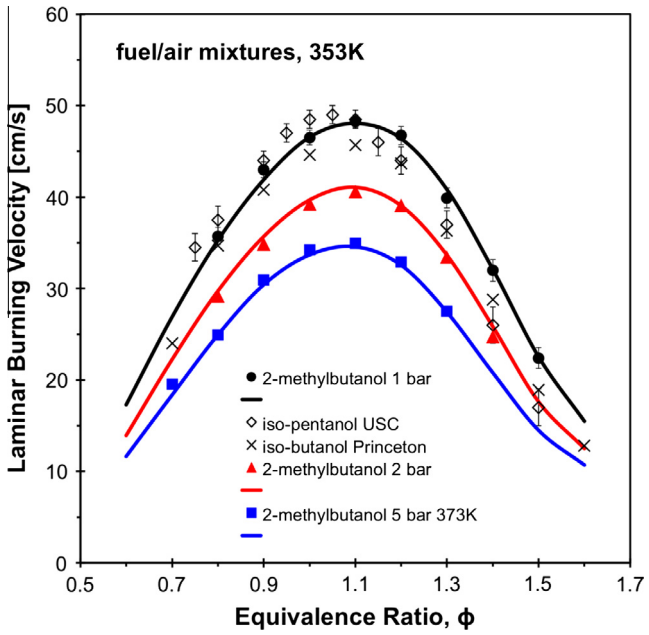

Fig. 12. Laminar flame speeds at unburnt gas temperature of 353 K (373 K for 5 bar) and different pressures. Experimental data (symbols) are compared to calculations (lines). Experimental data for iso-pentanol [31] and iso-butanol [51] are also presented.

and *iso*-pentanol under fuel-rich conditions, and the underlying cause of this difference could be from the intermediate production rate of *iso*-butene leading to the formation of unreactive *iso*-butenyl radical. The 2-methylbutanol flame does not produce as much *iso*-butene as *iso*-butanol and *iso*-pentanol. The proposed model is in satisfactory agreement with experimental data at all equivalence ratios and pressure conditions.

4.3. Jet-stirred reactor speciation

Recently, Serinyel et al. [33] measured concentration profiles of 2-methylbutanol oxidation in a jet-stirred reactor (JSR) at 10 atm, constant residence time, τ, of 0.7 s, over a temperature range of 700–1200 K, and equivalence ratios of 0.5, 1.0, 2.0, and 4.0. The present model is tested against the JSR data for an equivalence ratio of 1.0 since previous studies [53,54] have shown that the validation at these conditions is representative of the model's ability to reproduce experiments at other equivalence ratios. Simulations were conducted using the perfectly stirred reactor code in CHEMKIN PRO [45]. The model's ability to reproduce the data is considered good if the model closely matches the shape of experimental data, and if the simulated maximum mole fraction is within a factor 2 of the measured maximum mole fraction. Figure 13 presents the comparisons of reactants (2-methylbutanol and O_2), products (CO, CO_2, H_2 and H_2O), and major intermediate species (ethylene, propene, 1-butene, 2-butene, 2-methylbutene, formaldehyde, etc.). Fuel consumption begins around 770 K and is completely consumed around 950 K. The present model captures the fuel consumption behavior. Fuel is converted rapidly to major intermediate species such as 2-methylbutanal, formaldehyde, propanal, ethylene, and butene isomers (1-butene, 2-butene). The present model shows good agreement with experimental data for these intermediate species. The concentration profiles of reactants of fuel and O_2 and major products CO, CO_2 and H_2O are accurately reproduced, while H_2 is under-estimated under high temperature conditions ($T > 1000$ K). The under-estimation of H_2 for the stoichiometric mixture was also observed by Serinyel et al., but agreement was better at the other equivalence ratios [33]. Overall, the profile shape and maximum mole fractions of major intermediate species are well reproduced by the model, while ethylene is slightly under-estimated at temperatures ranging from 900 to 1200 K. Among oxygenated species, the maximum mole fraction of acetaldehyde is under-estimated by a factor of 2.5. The model also accurately captures the 2-methylbutanal profiles, which is produced mainly from the reaction of α-hydroxypentyl radical with O_2 at lower temperatures.

5. Conclusions

A new detailed kinetic model for 2-methylbutanol was compared against new and existing experimental data in shock tubes, premixed flames, and jet stirred reactors. The model was developed using methods established previously for the butanol and pentanol isomers, including comprehensive low- and high-temperature reaction pathways.

Shock tube ignition delay times were measured using the high-pressure shock tube (HPST) at KAUST for 2-methylbutanol/air mixtures at equivalence ratios of 0.5, 1.0, and 2.0, at temperatures from 750 to 1250 K, and at nominal pressures of 20 and 40 bar. The ignition delay times of 2-methylbutanol/air mixtures at intermediate temperatures are similar to those of *iso*-pentanol, while the reactivity of 2-methylbutanol is higher than *iso*-pentanol in the high temperature region. This trend is consistent with high-temperature shock tube ignition data at 1 atm [24]. The model reproduces shock tube ignition delay times at various pressures and temperatures. The present model included the reactions of internal H-atom migration from the OH group [39,40] and water elimination from QOOH [42], and their contributions on low-temperature oxidation of 2-methylbutanol were discussed using reaction path

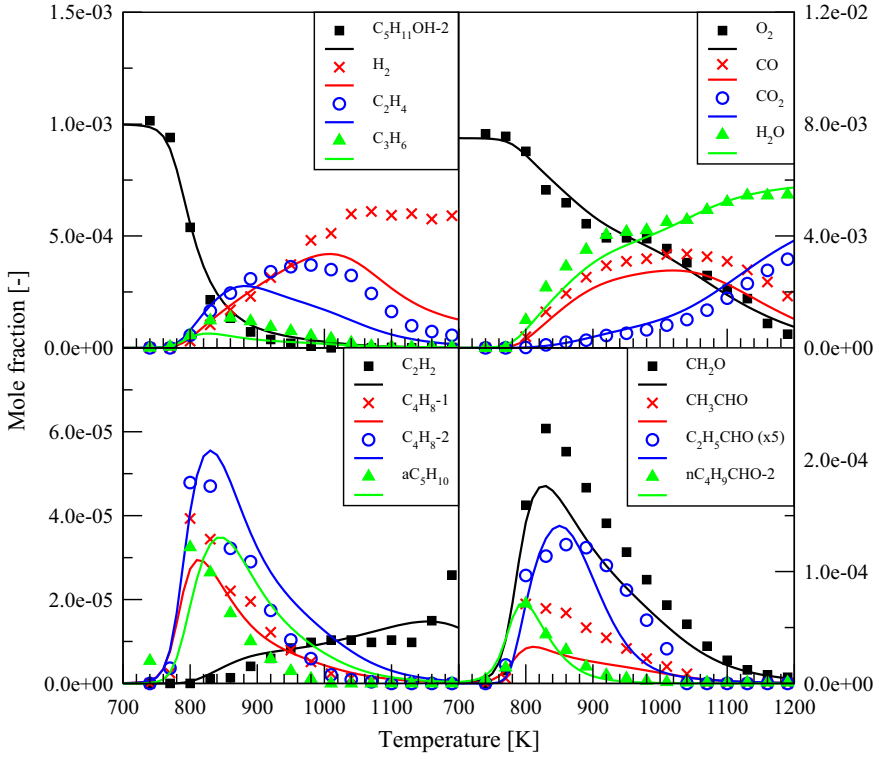

Fig. 13. 2-methylbutanol oxidation in a JSR at 10 atm, $t = 0.7$ s and $\phi = 1.0$. The initial fuel mole fraction was 0.1%. Experimental data [33] (symbols) are compared to calculations (lines).

analysis. Premixed laminar flame speeds were obtained using the spherically propagating flame configuration at pressures of 1, 2, and 5 bar. Laminar flame speeds of 2-methylbutanol are similar to those of *iso*-butanol and *iso*-pentanol and the results are consistent with experimentally and computationally observed flame speeds of *n*-alkanes having similar structure [52]. The model accurately reproduces flame speed data at various pressures and unburnt temperature conditions. JSR speciation simulations were also in reasonable agreement with experimental data from [33].

The proposed chemical kinetic model qualitatively and quantitatively reproduces a wide range of experimental data. Despite this progress, further fundamental chemical kinetic studies are needed for larger alcohols. Although the model displays satisfactory agreement with various combustion data, the reaction pathways and rate constants employed need to be confirmed via direct rate measurements or high-level quantum chemical/master equation calculations. In particular, a comprehensive theoretical study for various channels on R + O_2 potential energy surface is needed to determine low temperature reaction rate rules for alcohol fuels, as was done for alkane fuels [55,56]. Such studies will improve the model's predictive capabilities at a wider range of conditions, including high-pressure, low-temperature, and lean equivalence ratio conditions of relevance to advanced high-efficiency, low-emission engine technologies.

Acknowledgment

The authors acknowledge funding support from the Clean Combustion Research Center at King Abdulah University of Science and Technology (KAUST).

Appendix A. Supplementary material

Supplementary data associated with this article can be found, in the online version, at http://dx.doi.org/10.1016/j.combustflame.2015.01.014.

References

[1] S.M. Sarathy, P. Oßwald, N. Hansen, K. Kohse-Höinghaus, Prog. Energy Combust. Sci. 44 (2014) 40–102.
[2] A. Agarwal, Prog. Energy Combust. Sci. 33 (2007) 233–271.
[3] J.T. Moss, A.M. Berkowitz, M.A. Oehlschlaeger, J. Biet, V. Warth, P.A. Glaude, F. Battin-Leclerc, J. Phys. Chem. A 112 (2008) 10843–10855.
[4] S.M. Sarathy, M.J. Thomson, C. Togbé, P. Dagaut, F. Halter, C. Mounaim-Rousselle, Combust. Flame 156 (2009) 852–864.
[5] G. Black, H.J. Curran, S. Pichon, J.M. Simmie, V. Zhukov, Combust. Flame 157 (2010) 363–373.
[6] P. Dagaut, S.M. Sarathy, M.J. Thomson, Proc. Combust. Inst. 32 (2009) 229–237.
[7] K. Kohse-Höinghaus, P. Oßwald, T.A. Cool, T. Kasper, N. Hansen, F. Qi, C.K. Westbrook, P.R. Westmoreland, Angew. Chem., Int. Ed. 49 (2010) 3572–3597.
[8] C. Togbé, A. Mzé-Ahmed, P. Dagaut, Energy Fuels 24 (2010) 5244–5256.
[9] R. Grana, A. Frassoldati, T. Faravelli, U. Niemann, E. Ranzi, R. Seiser, R. Cattolica, K. Seshadri, Combust. Flame 157 (2010) 2137–2154.
[10] P. Oβwald, H. Güldenberg, K. Kohse-Höinghaus, B. Yang, T. Yuan, F. Qi, Combust. Flame 158 (2011) 2–15.
[11] N. Hansen, M.R. Harper, W.H. Green, Phys. Chem. Chem. Phys. 13 (2011) 20262–20274.
[12] J.K. Lefkowitz, J.S. Heyne, S.H. Won, S. Dooley, H.H. Kim, F.M. Hass, S. Jahangirian, F.L. Dryer, Y. Ju, Combust. Flame 159 (2012) 968–978.
[13] S.M. Sarathy, S. Vranckx, K. Yasunaga, M. Mehl, P. Oβwald, W.K. Metcalfe, C.K. Westbrook, W.J. Pitz, K. Kohse-Höinghaus, R.X. Fernandes, H.J. Curran, Combust. Flame 159 (2012) 2028–2055.
[14] A. Frassoldati, R. Grana, T. Faravelli, E. Ranzi, P. Oßwald, K. Kohse-Höinghaus, Combust. Flame 159 (2012) 2295–2311.
[15] K. Yasunaga, T. Mikajiri, S.M. Sarathy, T. Koike, F. Gillespie, T. Nagy, J.M. Simmie, H.J. Curran, Combust. Flame 159 (2012) 2009–2027.
[16] J. Zhang, L. Wei, X. Man, X. Jiang, Y. Zhang, E. Hu, Z. Huang, Energy Fuels 26 (2012) 3368–3380.
[17] J. Cai, L. Zhang, F. Zhang, Z. Wang, Z. Cheng, W. Yuan, F. Qi, Energy Fuels 26 (2012) 5550–5568.
[18] S.S. Vasu, S.M. Sarathy, Energy Fuels 27 (2013) 7072–7080.
[19] J. Cai, W. Yuan, L. Ye, Z. Cheng, Y. Wang, L. Zhang, F. Zhang, Y. Li, F. Qi, Combust. Flame 160 (2013) 1939–1957.
[20] N. Hansen, S.S. Merchant, M.R. Harper, W.H. Green, Combust. Flame 160 (2013) 2343–2351.
[21] C. Togbé, F. Halter, F. Foucher, C. Mounaim-Rousselle, P. Dagaut, Proc. Combust. Inst. 33 (2011) 367–374.
[22] L. Zhao, L. Ye, F. Zhang, L. Zhang, J. Phys. Chem. A 116 (2012) 9238–9244.
[23] K.A. Heufer, S.M. Sarathy, H.J. Curran, A.C. Davis, C.K. Westbrook, W.J. Pitz, Energy Fuels 26 (2012) 6678–6685.
[24] C. Tang, L. Wei, X. Man, J. Zhang, Z. Huang, C.K. Law, Combust. Flame 160 (2013) 520–529.
[25] Q. Li, E. Hu, X. Zhang, Y. Cheng, Z. Huang, Energy Fuels 27 (2013) 1141–1150.
[26] L. Wei, C.S. Cheung, Z. Huang, Energy (2014) 172–180.
[27] Y. Yang, J.E. Dec, N. Dronniou, B. Simmons, SAE Int. J. Fuels Lubricants 3 (2010) 725–741.
[28] T. Tsujimura, W.J. Pitz, Y. Yang, J.E. Dec, SAE Int. J. Fuels Lubricants 4 (2011) 257–270.
[29] G. Dayma, C. Togbé, P. Dagaut, Energy Fuels 25 (2011) 4986–4998.
[30] T. Tsujimura, W.J. Pitz, F. Gillespie, H.J. Curran, B.W. Weber, Y. Zhang, C.-J. Sung, Energy Fuels 26 (2012) 4871–4886.
[31] S.M. Sarathy, S. Park, B.W. Weber, W. Wang, P.S. Veloo, A.C. Davis, C. Togbé, C.K. Westbrook, O. Park, G. Dayma, Z. Luo, M.A. Oehlschlaeger, F.N. Egolfopoulos, T. Lu, W.J. Pitz, C.-J. Sung, P. Dagaut, Combust. Flame 160 (2013) 2712–2728.
[32] Q. Li, E. Hu, Y. Cheng, Z. Huang, Fuel 112 (2013) 263–271.
[33] Z. Serinyel, C. Togbé, G. Dayma, P. Dagaut, Combust. Flame 161 (2014) 3003–3013.
[34] X. Zhang, B. Yang, W. Yuan, Z. Cheng, L. Zhang, Y. Li, F. Qi, Proc. Combust. Inst. 35 (2015) 409–417.
[35] A. Lucassen, S. Park, N. Hansen, S.M. Sarathy, Proc. Combust. Inst. 35 (2015) 813–820.
[36] A.F. Cann, J.C. Liao, Appl. Microbiol. Biotechnol. 81 (2008) 89–98.
[37] C.R. Shen, J.C. Liao, Energy Environ. Sci. 5 (2012) 9574–9583.
[38] C.-W. Zhou, S.J. Kippenstein, J.M. Simmie, H.J. Curran, Proc. Combust. Flame 34 (2013) 501–509.
[39] D.J.M. Ray, D.J. Waddington, Combust. Flame 20 (1973) 327–334.
[40] M.I. Sway, D.J. Waddington, J. Chem. Soc., Perkin Trans. 2 (1983) 139–143.
[41] O. Welz, J. Zádor, J.D. Savee, M.Y. Ng, G. Meloni, R.X. Fernandes, L. Sheps, B.A. Simmons, T.S. Lee, D.L. Osborn, C.A. Taatjes, Phys. Chem. Chem. Phys. 14 (2012) 3112–3127.
[42] O. Welz, S.J. Klippenstein, L.B. Harding, C.A. Taatjes, J. Zádor, J. Phys. Chem. Lett. 4 (2013) 350–354.
[43] E. Ritter, J. Bozzelli, Int. J. Chem. Kinet. 23 (1991) 767–778.
[44] L.S. Tee, S. Gotoh, W.E. Stewart, Ind. Eng. Chem. Fund. 5 (1966) 356–363.
[45] CHEMKIN-PRO 15112, Reaction Design, San Diego, 2011.
[46] C. Prathap, A. Ray, M.R. Ravi, Combust. Flame 155 (2008) 145–160.
[47] M. Chaos, F.L. Dryer, Int. J. Chem. Kinet. 42 (2010) 143–150.
[48] K.P. Somers, J.M. Simmie, F. Gillespie, U. Burke, J. Connolly, W.K. Metcalfe, F. Battin-Leclerc, P. Dirrenberger, O. Herbinet, P.-A. Glaude, H.J. Curran, Proc. Combust. Inst. 34 (2013) 225–232.
[49] W.K. Metcalfe, S.M. Burke, S.S. Ahmed, H.J. Curran, Int. J. Chem. Kinet. 45 (2013) 638–675.
[50] G. da Silva, J.W. Bozzelli, L. Liang, J.T. Farrell, J. Phys. Chem. A 113 (2009) 8923–8933.
[51] W. Liu, A.P. Kelley, C.K. Law, Proc. Combust. Inst. 33 (2011) 995–1002.
[52] C. Ji, E. Dames, Y.L. Wang, H. Wang, F.N. Egolfopoulos, Combust. Flame 157 (2010) 277–287.
[53] S. Gaïl, M.J. Thomson, S.M. Sarathy, S.A. Syed, P. Dagaut, P. Diévart, A.J. Marchese, F.L. Dryer, Proc. Combust. Inst. 31 (2007) 305–311.
[54] S. Gaïl, S.M. Sarathy, M.J. Thomson, P. Diévart, P. Dagaut, Combust. Flame 155 (2008) 635–650.
[55] S.M. Villano, L.K. Huynh, H.-H. Carstensen, A.M. Dean, J. Phys. Chem. A 115 (2011) 13425–13442.
[56] S.M. Villano, L.K. Huynh, H.-H. Carstensen, A.M. Dean, J. Phys. Chem. A 116 (2012) 5068–5089.